Original

Beckmann, F.; Hammel, J.; Moosmann, J.; Lottermose, L.; Gunnell, G.; Habersetzer, J.:

Optimization of high-energy microtomography using synchrotron radiation at PETRA III.

In: Müller, B.; Wang, G. (eds.): Proceedings of SPIE. Vol. 111131 Bellingham, Wash.: SPIE, 2019. 111131A-1 - 111131A-8.
First published online by SPIE: 08.10.2019

https://dx.doi.org/10.1117/12.2530001

PROCEEDINGS OF SPIE

SPIEDigitalLibrary.org/conference-proceedings-of-spie

Optimization of high-energy microtomography using synchrotron radiation at PETRA III

Beckmann, Felix, Hammel, Jörg, Moosmann, Julian, Lottermoser, Lars, Gunnell, Gregg, et al.

Felix Beckmann, Jörg U. Hammel, Julian Moosmann, Lars Lottermoser, Gregg F. Gunnell, Jörg Habersetzer, "Optimization of high-energy microtomography using synchrotron radiation at PETRA III," Proc. SPIE 11113, Developments in X-Ray Tomography XII, 111131A (8 October 2019); doi: 10.1117/12.2530001

SPIE.

Event: SPIE Optical Engineering + Applications, 2019, San Diego, California, United States

Optimization of high-energy microtomography using synchrotron radiation at PETRA III

Felix Beckmann*[a], Jörg. U. Hammel[a], Julian Moosmann[a], Lars Lottermoser[a], Greg F. Gunnell[†b], Jörg Habersetzer[c]
[a]Institute of Materials Research, Helmholtz-Zentrum Geesthacht, 21502 Geesthacht, Germany;
[b]Devision of Fossil Primates, Duke Lemur Center, Duke University, Durham, NC 27705, USA;
[c]Abteilung Messelforschung, Senckenberg Forschungsinstitut, 60325 Frankfurt am Main, Germany

ABSTRACT

Microtomography using synchrotron radiation has proven to be a valuable tool for characterizing samples within biology, medical science, paleontology and materials science. A variety of attenuation contrast and phase-contrast imaging techniques were established to focus on spatial resolution, density resolution, and temporal resolution. In this paper, we focus on the recent developments at beamline P07 at PETRA III, Hamburg, Germany, for high-energy microtomography to provide high-density resolution for the study of a fossil tooth sample. Due to the integration of two independent CCDs for alternating use within the X-ray detector the imaging throughput was doubled. The concept, the alignment process, and first results are presented.

Keywords: Computed tomography, synchrotron radiation, density resolution, attenuation contrast, fossil tooth

1. INTRODUCTION

The Helmholtz-Zentrum Geesthacht, Germany, is operating the user experiments for microtomography at the beamlines P05 and P07 using synchrotron radiation (SR) produced in the storage ring PETRA III at DESY, Hamburg, Germany. Attenuation-contrast and phase-contrast techniques were established to provide an imaging tool for applications in biology,[1-3] medical science,[4-8] paleontology,[9-11] and materials science.[12-15] The high intense and low divergent SR allows for the use of an X-ray monochromator to monochromatize the white spectrum to a bandwidth $\Delta E/E$ of 10^{-2} to 10^{-4} depending on the type of monochromator. This results in nearly artefact free tomograms showing a high-spatial resolution. Depending on the requirements of the investigated samples the measurement parameters and setup can be optimized for high-temporal resolution[16, 17] or high-density resolution. The density resolution, which represents the ability to differentiate material densities or material compositions, mainly depends on the applied contrast and the photon statistics. For phase contrast, the photon statistics of the X-ray detector is less important,[18] but for attenuation contrast the density resolution strongly depends on the photon statistics of the X-ray detector.[19] By the use of a CCD instead of a CMOS sensor we focus on the statistical response instead on the temporal resolution of the system. As the readout of the CCD-based X-ray detector requires a significant part of the scan time, we integrate two independent CCD sensors. By the fast movement of a visible light mirror we switch to the second sensor during the readout of the first sensor and directly start the exposure of the second sensor for obtaining the next projection. This approach allows for doubling the imaging throughput. The microtomography setup and the alignment process for the X-ray detector is shown in Section 2. First results using this system for the characterization of a fossil tooth sample is presented in Section 3.

2. SETUP AND ALIGNMENT

In Figure 1, the setup for microtomography located in the Experimental Hutch 4 of the high-energy materials-science beamline P07 at PETRA III is shown. The main components of the system are an X-ray detector, a sample manipulation stage and a substructure. The robust substructure allows for precise alignment of the total system to the X-ray beam (movement and tilt). The sample manipulation stage consists of a high-precision air-bearing rotation, an air-bearing translation for the sample movement perpendicular to the X-ray beam, and three vertical translation stages for precise alignment in z-direction and tilting around x/y axes. Within the rotation axis, the sample can be positioned and tilted

*Corresponding author: felix.beckmann@hzg.de

Developments in X-Ray Tomography XII, edited by Bert Müller, Ge Wang, Proc. of SPIE Vol. 11113, 111131A · © 2019 SPIE
CCC code: 0277-786X/19/$21 · doi: 10.1117/12.2530001

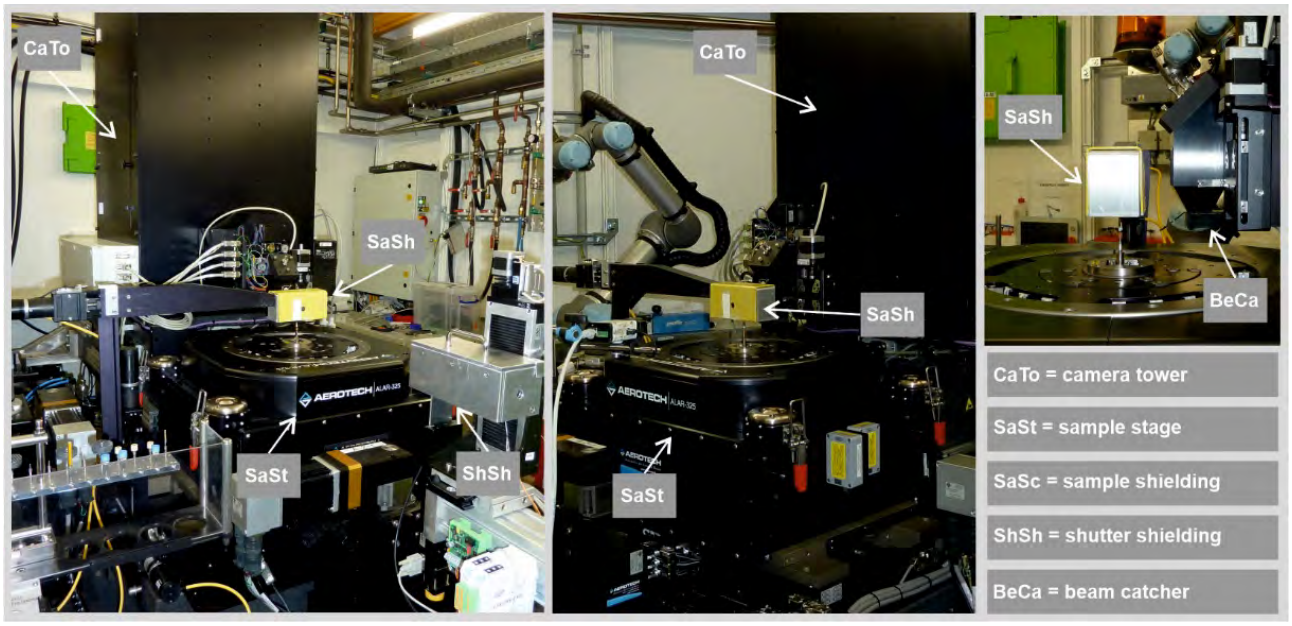

Figure 1. Experimental setup for microtomography at beamline P07 at PETRA III. Several X-ray shields were included to protect the pixel detectors from the scattered radiation. In front of the apparatus, an X-ray shutter and a beam intensity monitor are installed, which require a permanent shielding (ShSh). During the scan, the scattering of the sample will be catched by a movable shielding (SaSh). For automatic sample changes the camera tower (CaTo) and the sample shielding (SaSh) has to be placed to a rest position. The sample changer is shown in the background of the middle picture. For high photon-energies the X rays are only partly attenuated by the luminescent screen. The transmitted X-rays are then absorbed by the beam catcher (BeCa) directly installed behind the first mirror of the optical system as shown in the right image.

relative to the rotation axis. The X-ray detector is built by a luminescent screen to convert the X rays into visible light. This image is then magnified by a microscope lens system onto the CCD or CMOS detector. More information about the used components and a more detailed description of the system can be found elsewhere.[20-22]

Table 1. Mechanical components of the sample manipulation stage

Rotation:	ABRT-260	Air-Bearing Direct-Drive Rotary Stage (70 nm wobble), AEROTECH, Inc., USA
Translation:	ABL800010-XLC	Air-Bearing Direct-Drive Linear Stage (150 nm precision), AEROTECH, Inc., USA
Alignment:	3 x ATSLC-100	Linear Stage (*z*-direction) (1 µm precision), AEROTECH, Inc., USA
Within axis:	sample *x*/*y*/*z* + tilt	Attocube ANP/ANG Piezo Stick-Slip Stages, attocube systems AG, Germany

Table 2. Mechanical components of the optical system

Translation camera tower:	Air-Bearing Direct-Drive Linear Stage, micos (now PI miCos GmbH), Germany
Microscope-Lens-System:	Focus-Objective, POG GmbH, Germany Tubus-Objectives, magnification 5×/10×/20×/40×, NA=0.2, POG GmbH, Germany
Movement Mirror B:	Piezo Stick-Slip Stage, SmarAct GmbH, Germany
Movement Mirror A:	ANT95L, Single-Axis Linear Direct-Drive Nanopositioning Stage, AEROTECH, Inc.

Table 3. Parameters of the CCD camera A and B

Supplier:	EHD imaging GmbH, Germany
System:	SciCam SC09000M, USB2.0, liquid cooling
Sensor:	Kodak, KAF-09000, pixels: 3056 × 3056, pixel size: 12 µm, operating temperature: -15 °C
Readout:	8 MHz, 16 bit, single readout, measured frame rate: 0.3 1/s

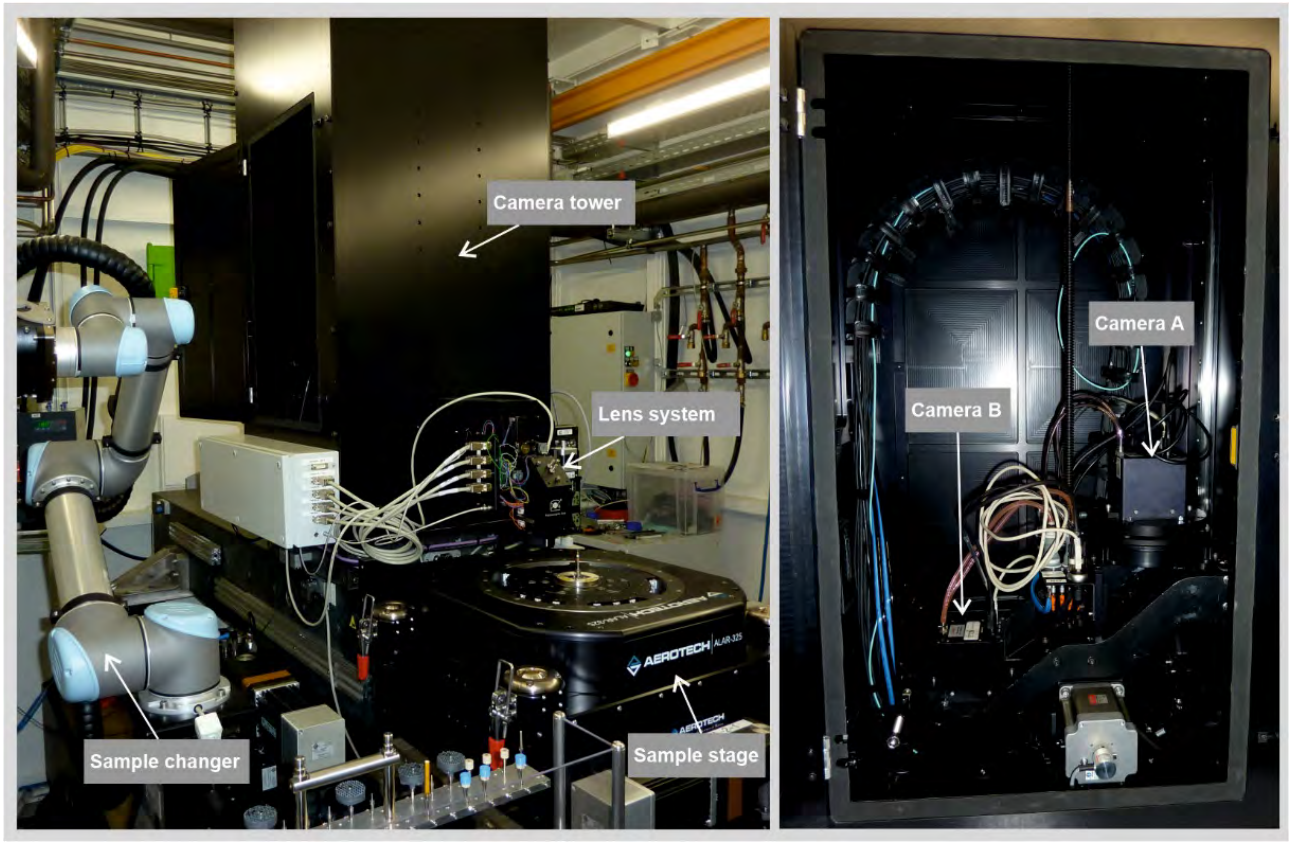

Figure 2. Experimental setup at beamline P07 at PETRA III. Within the camera tower two imaging sensors are installed (Camera A and Camera B). For changing the optical magnification, both cameras together can be lifted by a vertical travel.

Herein, we focus on the recent enhancements within the X-ray detector, see Figures 2 and 3, and the improvement of the shielding to catch scattered X rays and protect the camera systems from high energy photon hits, cp. Figure 1. The main mechanical components installed are listed in Tables 1 and 2. Within the camera tower two CCD cameras of the same type are installed. By the movement of mirror A, each camera system can be selected. On the right images in Figure 3, both positions are shown. In Table 3, the parameters of the used CCD systems are given.

2.1 Coarse alignment without X-ray beam

By using an alignment laser within the X-ray beam path (luminescent screen and cameras deinstalled), the tilts of the mirror systems are adjusted. Then, the cameras and a visible test pattern at the position of the luminescent screen are installed. The rotation of the camera around the optical axis and the position of the cameras in z direction together with the position of mirror B are adjusted.

2.2 Fine alignment with X-ray beam

For the experiment, we selected a photon energy of 60 keV and installed a 100 µm-thick $CdWO_4$ luminescent screen. The optical system is focused by the optimization of the modulated transfer function (MTF) calculated from a measurement of an edge projection. Then, the optical magnification is carefully measured by the precise movement of the used edge. This is done independently for camera A and camera B. By changing the position of mirror B and the z-position of the cameras the focusing measurement is repeated until the position of the focus lens and the measured magnification match. Therefore, the effective pixel size of the two cameras are the same and during the experiment the only required movement to switch between camera A and camera B is the positioning of mirror A.

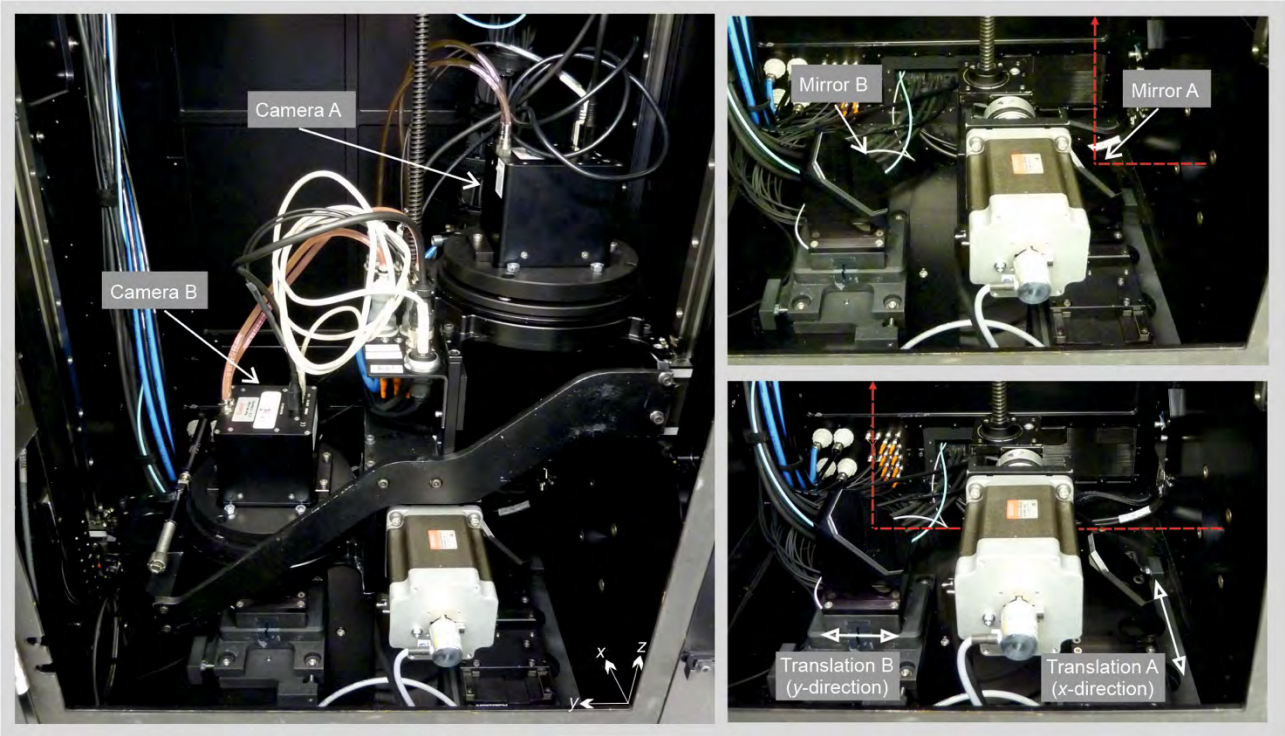

Figure 3. The different components used for alignment of the optical beam path for the use of the two CCD cameras are shown. Both cameras can be lifted by a motorized vertical travel up to 600 mm. Each camera can be lifted up to 3 mm, independently. The position of mirror B can be fine adjusted in *y*-direction by a piezo stage up to 1 mm. Mirror A can be moved out of the beam, see red-colored dashed line with arrow head by a translation in *x*-direction.

3. EXPERIMENT AND RESULTS

The tomographic experiment was performed at P07 in high beta mode. The undulator spectrum was monochromatized to a photon energy of about 60 keV by a double-crystal bent-Laue monochromator. At the sample position, the X-ray beam size was about 2.5 × 2.5 mm². The measured effective pixel size of the X-ray detector was 1.336 µm. The exposure time for one projection was 90 ms. The sample-detector distance was 80 mm. Several sets of flat fields are taken within the scan to cope with intensity changes in the beam profile, which are due to the heat load of the white X-ray beam onto the first crystal of the monochromator.

3.1 Single-CCD and Dual-CCD measurement of test sample

For setting up the measurement for dual CCD use and to demonstrate and verify the reconstruction pipeline, tomographic scans of a miniature lamp were performed. The sample composition was well suited for imaging test experiments using high photon energies. Using the CCD A, a tomographic scan consisting of 1201 projections over 2π was performed. The sequence of the images were ten dark, three flat fields, 200 projections, three flat fields, and so on. The number of images taken was 1231 resulting in a total scan time of 71 minutes. Then, the measurement was repeated using camera A and camera B. During the readout of the one camera, the mirror B was moved to select the other camera. Again 1201 projections over 2π were taken. The sequence of the images were 20 dark (a,b), six flat fields (a,b), 200 projections (a,b), six flat fields (a,b), and so on. In total 1262 images were taken resulting in a total scan time of 36 minutes.

For reconstruction of the dual CCD measurement, we first reconstructed the subset for camera A and B, separately. The registration of the two volumes shows that no scaling, no rotation , no horizontal shift, but a vertical shift of 27 pixels was required. Taking this shift into account the reconstruction was performed using a raw binning of two. In Figure 4, slices and a 3D rendering of the reconstructed volume using both cameras are presented.

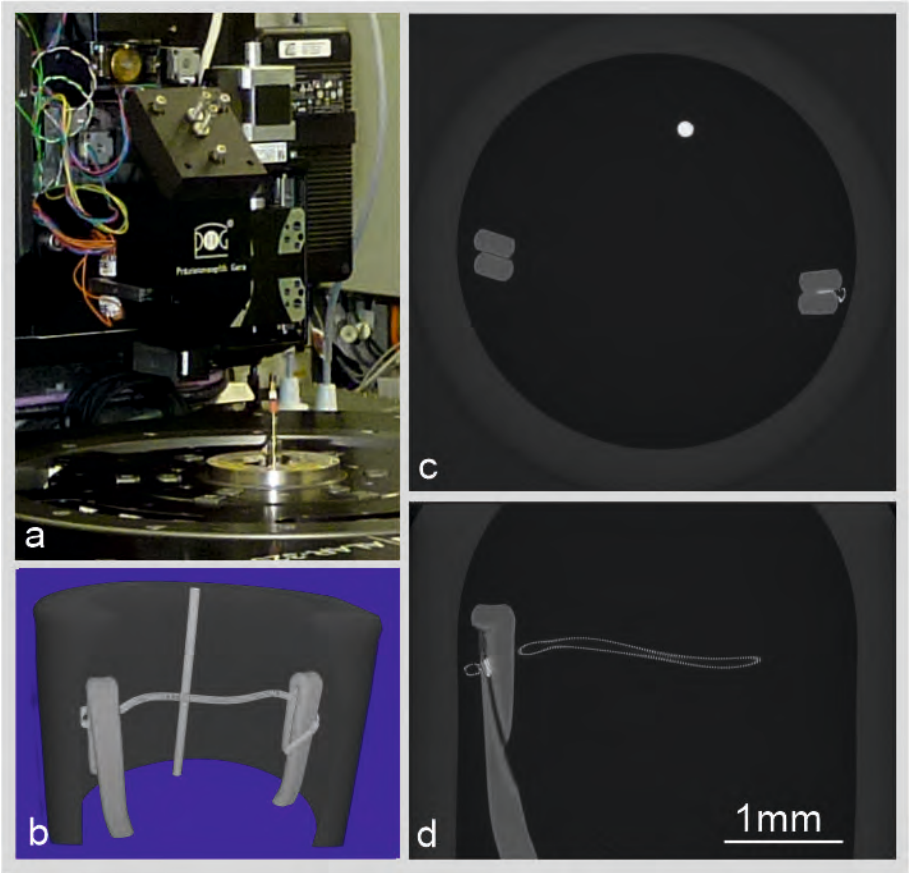

Figure 4. Tomographic scan of a miniature lamp using the dual-CCD setup. The installed multi-component sample is shown in a. Selected reconstructed slices are presented in c and d. The volume rendering is represented in part b.

3.2 Dual-CCD measurement of a fossil tooth

The aim of the investigation of a fossil tooth using synchrotron radiation-based microtomography was to study the enamel in high-density resolution. This probably allows for capturing the incremental growth lines in teeth of *Aegyptopithecus* from the fossil site Fayum, Egypt. This could make it possible examining how teeth developed through ontogeny in early anthropoid primates representing even months or weeks in the individual development of particular teeth. The scanned specimen shown in Figure 5 is a deciduous premolar (dP4) of *Aegyptopithecus*, Fossil No. 3057 (Quarry M - Field No. 82-525).

The sample was placed into an Eppendorf tube and fixed by cotton wool. As the sample was larger than the available field of view (FOV) provided by the X-ray beam, tomographic scans at two lateral and five vertical positions were performed. For each of the five heights, 2,499 images were taken. The total scan time was 6 hours, which is half of the required scan time by the use of only one CCD camera. Before reconstruction, the related images were combined to build a single tomographic scan consisting of 1,201 projections of 2π. To increase the density resolution in the tomogram, a raw binning of four is used resulting in a volume of 1,237 × 1,237 × 1,725 voxels and 6.6 × 6.6 × 9.2 mm³, respectively.[23] In Figure 5, a series of reconstructed slices through the total volume is shown.

4. SUMMARY AND OUTLOOK

The use of two slow-scan CCD devices with alternating use during the tomographic scans allows for doubling the imaging throughput of the present microtomography system at beamline P07 at PETRA III. This upgraded experimental setup was successfully applied to characterize the enamel/dentin boundary and histological details in a tooth of *Aegyptopithecus* from the fossil site Fayum, Egypt. The data evaluation is ongoing to reveal incremental growth lines on the basis of sub-volumes reconstructed by using a raw binning of two with a voxel size of 2.672 µm showing a higher spatial resolution. A detailed

comparison comparing the used CCD devices with actual CMOS sensors is ongoing. The comparison will be based on the measurement of the photon transfer curve,[24] the simulation of the experiment,[25] and the measurement of a phantom test sample.

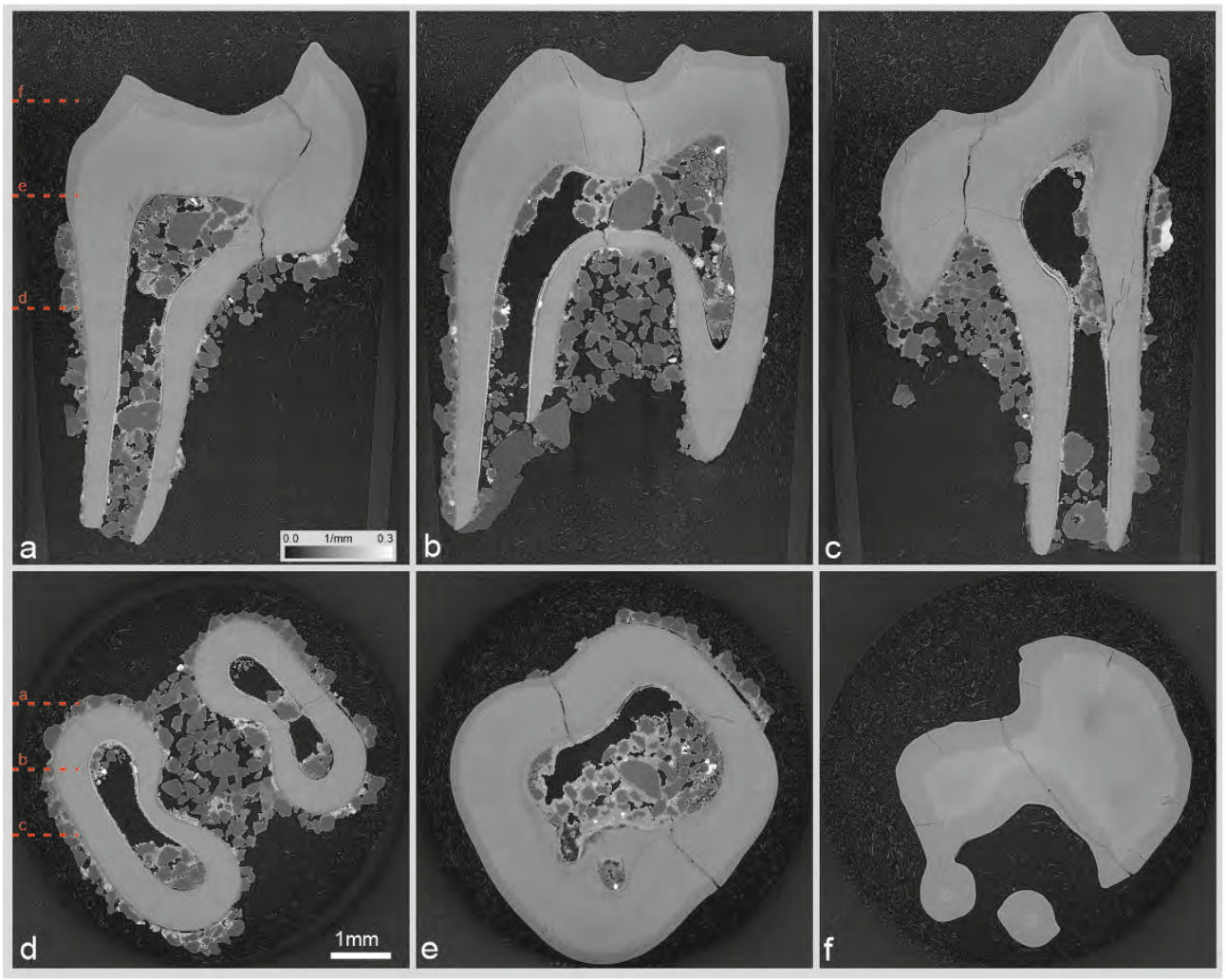

Figure 5. High-energy microtomography scan of a tooth of *Aegyptopithecus* from the fossil site Fayum, Egypt. Reconstructed slices (d,e,f) and vertical-calculated slices (a,b,c) through the total-reconstructed volume are shown. The position of the virtual cuts are marked in red color in parts a and d. The investigation was performed using a photon energy of 60 keV at the beamline P07 at PETRA III.

ACKNOWLEDGEMENTS

The authors like to thank Hilmar Burmester and Jens Brehling for the technical support at the beamline P07. The experiment was performed using SR at PETRA III within the beamtime ID 11005744.

REFERENCES

[1] Ziegler, A., Neues, F., Janáček, J., Beckmann, F., and Epple, M., "Mineral in skeletal elements of the terrestrial crustacean Porcellio scaber: SRμCT of function related distribution and changes during the moult cycle," Arthropod Structure and Development, 46(1), 63-76 (2017).

[2] Lautner, S., Lenz, C., Hammel, J., Moosmann, J., Kühn, M., Caselle, M., Vogelgesang, M., Kopmann, A., and Beckmann, F., "Using SRμCT to define water transport capacity in Picea abies." Proc. SPIE 10391, 1039118 (2017).

[3] Schmelzle, S., Heethoff, M., Heuveline, V., Lösel, P., Becker, J., Beckmann, F., Schluenzen, F., Hammel, J. U., Kopmann, A., Mexner, W., Vogelgesang, M., Jerome, N. T., Betz, O., Beutel, R., Wipfler, B., Blanke, A., Harzsch, S., Hörnig, M., Baumbach, T., and Van De Kamp, T., "The NOVA project: Maximizing beam time efficiency through synergistic analyses of SRμCT data." Proc. SPIE 10391, 103910P (2017).

[4] Buscema, M., Hieber, S., Schulz, G., Deyhle, H., Hipp, A., Beckmann, F., Lobrinus, J. A., Saxer, T., and Müller, B., "Ex vivo evaluation of an atherosclerotic human coronary artery via histology and high-resolution hard X-ray tomography," Scientific Reports, 9, 14348 (2019).

[5] Bikis, C., Rodgers, G., Deyhle, H., Thalmann, P., Hipp, A., Beckmann, F., Weitkamp, T., Theocharis, S., Rau, C., Schulz, G., and Müller, B., "Sensitivity comparison of absorption and grating-based phase tomography of paraffin-embedded human brain tissue," Applied Physics Letters, 114(8), 083702 (2019).

[6] Dziadowiec, I., Beckmann, F., Schulz, G., Deyhle, H., and Müller, B., "Characterization of a human tooth with carious lesions using conventional and synchrotron radiation-based micro computed tomography." Proc. SPIE 9212, 92120W (2014).

[7] Graef, F., Richtert, R., Fetz, V., Murgia, X., De Rossi, C., Schneider-Daum, N., Allegretta, G., Elgaher, W., Hauipenthal, J., Empting, M., Beckmann, F., BroEnstrup, M., Hartmann, R., Gordon, S., and Lehr, C. M., "In Vitro Model of the Gram-Negative Bacterial Cell Envelope for Investigation of Anti-Infective Permeation Kinetics," ACS Infectious Diseases, 4(8), 1188-1196 (2018).

[8] Beckmann, F., Dziadowiec, I., Lottermoser, L., Thalmann, P., Herzen, J., Greving, I., Schulz, G., Hieber, S. E., and Müller, B., "High-energy microtomography using synchrotron radiation at PETRA III / DESY for the 3D characterization of caries lesions," European Cells and Materials, 28, 23 (2014).

[9] Castanhinha, R., Araújo, R., Júnior, L. C., Angielczyk, K. D., Martins, G. G., Martins, R. M. S., Chaouiya, C., Beckmann, F., and Wilde, F., "Bringing dicynodonts back to life: Paleobiology and anatomy of a new emydopoid genus from the Upper Permian of Mozambique," PLoS ONE, 8(12), e80974 (2013).

[10] Pohl, H., Wipfler, B., Grimaldi, D., Beckmann, F., and Beutel, R. G., "Reconstructing the anatomy of the 42-million-year-old fossil †mengea tertiaria (Insecta, Strepsiptera)," Naturwissenschaften, 97(9), 855-859 (2010).

[11] Habersetzer, J., Scherf, H., Beckmann, F., and Seidel, R.,"3-D animation of total skeletons and microtomographic details of fossils from the pit at Messel", CFS Courier Forschungsinstitut Senckenberg, Issue 252, 237-241 (2004).

[12] Zeller-Plumhoff, B., Helmholz, H., Feyerabend, F., Dose, T., Wilde, F., Hipp, A., Beckmann, F., Willumeit-Römer, R., and Hammel, J. U., "Quantitative characterization of degradation processes in situ by means of a bioreactor coupled flow chamber under physiological conditions using time-lapse SRμCT," Materials and Corrosion, 69(3), 298-306 (2018).

[13] Willumeit-Römer, R., Moosmann, J., Zeller-Plumhoff, B., Florian Wieland, D. C., Krüger, D., Wiese, B., Wennerberg, A., Peruzzi, N., Galli, S., Beckmann, F., and Hammel, J. U.,"Visualization of implant failure by synchrotron tomography", Minerals, Metals and Materials Series, Part F12, 275-284 (2018).

[14] Reinke, S. K., Wilde, F., Kozhar, S., Beckmann, F., Vieira, J., Heinrich, S., and Palzer, S., "Synchrotron X-Ray microtomography reveals interior microstructure of multicomponent food materials such as chocolate," Journal of Food Engineering, 174, 37-46 (2016).

[15] Nellesen, J., Abdulgader, M., Tillmann, W., and Beckmann, F., "3D mu CT and SEM Analysis of Resolidified Tips of Cored Wires Used in Twin-Wire Arc Spraying," Journal of Thermal Spray Technology, 24(1-2), 55-62 (2015).

[16] Vegso, K., Wu, Y. L., Takano, H., Hoshino, M., and Momose, A., "Development of pink-beam 4D phase CT for in-situ observation of polymers under infrared laser irradiation," Scientific Reports, 9, 7404 (2019).

[17] Garcia-Moreno, F., Kamm, P. H., Neu, T. R., Bulk, F., Mokso, R., Schleputz, C. M., Stampanoni, M., and Banhar, J., "Using X-ray tomoscopy to explore the dynamics of foaming metal," Nature Communications, 10, 3762 (2019).

[18] Hipp, A., Herzen, J., Hammel, J. U., Lytaev, P., Schreyer, A., and Beckmann, F., "Single-grating interferometer for high-resolution phase-contrast imaging at synchrotron radiation sources." Proc. SPIE 9967, 996718 (2016).

[19] Beckmann, F.,"Neutron and Synchrotron-Radiation-Based Imaging for Applications in Materials Science - From Macro- to Nanotomography", Neutrons and Synchrotron Radiation in Engineering Materials Science: From Fundamentals to Applications: Second Edition, WILEY-VCH, 253-273 (2017).

[20] Haibel, A., Beckmann, F., Dose, T., Herzen, J., Ogurreck, M., Müller, M., and Schreyer, A., "Latest developments in microtomography and nanotomography at PETRA III," Powder Diffraction, 25(2), 161-164 (2010).

[21] Wilde, F., Ogurreck, M., Greving, I., Hammel, J. U., Beckmann, F., Hipp, A., Lottermoser, L., Khokhriakov, I., Lytaev, P., Dose, T., Burmester, H., Müller, M., and Schreyer, A., "Micro-CT at the imaging beamline P05 at PETRA III." AIP Conference Proceedings 1741, 030035 (2016).

[22] Greving, I., Wilde, F., Ogurreck, M., Herzen, J., Hammel, J. U., Hipp, A., Friedrich, F., Lottermoser, L., Dose, T., Burmester, H., Müller, M., and Beckmann, F., "P05 imaging beamline at petra III - First results." Proc. SPIE 9212, 92120O (2014).

[23] Thurner, P., Beckmann, F., and Müller, B., "An optimization procedure for spatial and density resolution in hard X-ray micro-computed tomography," Nuclear Instruments and Methods in Physics Research, Section B: Beam Interactions with Materials and Atoms, 225(4), 599-603 (2004).

[24] Lytaev, P., Hipp, A., Lottermoser, L., Herzen, J., Greving, I., Khokhriakov, I., Meyer-Loges, S., Plewka, J., Burmester, J., Caselle, M., Vogelgesang, M., Chilingaryan, S., Kopmann, A., Balzer, M., Schreyer, A., and Beckmann, F., "Characterization of the CCD and CMOS cameras for grating-based phase-contrast tomography." Proc. SPIE 9212, 921218 (2014).

[25] Otte, F., Faragó, T., Moosmann, J., Hipp, A. C., Hammel, J. U., and Beckmann, F., "Simulation framework SYRIS tested for microtomography applications at the imaging beamline P05/PETRA III." AIP Conference Proceedings 2054, 060084 (2019).